Quantum conductivity corrections in free-standing and supported $n^+$-GaAs wires



1990 J. Phys.: Condens. Matter 2 1807

(http://iopscience.iop.org/0953-8984/2/7/011)

J. Phys.: Condens. Matter **2** (1990) 1807–1815. Printed in the UK

# Quantum conductivity corrections in free-standing and supported n$^+$-GaAs wires

A Potts, D G Hasko, J R A Cleaver, C G Smith, H Ahmed, M J Kelly†, J E F Frost, G A C Jones, D C Peacock† and D A Ritchie

Cavendish Laboratory, Department of Physics, University of Cambridge, Madingley Road, Cambridge CB3 0HE, UK

Received 24 July 1989, in final form 25 October 1989

**Abstract.** Low-temperature electrical and magnetoresistance measurements have been performed on free-standing and supported wires of n-type GaAs doped to $10^{17}$ cm$^{-3}$ over the temperature range 0.47–4.2 K. These wires were triangular in cross-section, with widths of 600–900 nm and lengths of 3.2–10 $\mu$m. We report that the observed increase in the resistance for temperatures below 4.2 K can be interpreted as being due to a combination of weak localisation of 3D electron–electron interaction effects. We will also show how the results described here can be used as the basis for a determination of the phonon conductivity and dimensionality in free-standing structures.

## 1. Introduction

In addition to the quantum corrections to the electrical conduction that have been observed in systems such as doped wires on a substrate [1], MOSFET accumulation layers [2], heterojunctions [3, 4] and evaporated metal structures [5, 6], it has been predicted that free-standing structures should exhibit analogous effects in the conduction of phonons [7–9] in cases where the dimensionality of the phonons is restricted. Although this has been known for several years, progress in this area has been restricted by the limitations of device fabrication. Only recently with the availability of high resolution electron beam lithography, and the advent of molecular beam epitaxy (MBE) and silicon-on-insulator [10] (SOI) techniques has it been possible to fabricate sub-micrometre free-standing devices of single-crystal material on insulating [11] and semi-insulating [12] substrates. These structures are capable of exhibiting low-dimensional electronic and thermal transport. To this end, free-standing GaAs wires have been fabricated [12] with widths ranging from 100 nm to 1 $\mu$m, and lengths of up to 40 $\mu$m, in a MBE-grown layer with a silicon doping concentration of $10^{17}$ cm$^{-3}$ on a semi-insulating substrate. The wires in these structures have an inverted isosceles triangular cross-section (see figure 1) as a result of the particular fabrication process employed and consequently have a non-uniform width. The width to which we will refer therefore is that at the top of the wire. This, however, will differ considerably from the width of the conducting cross-section of the wire due to the combined effect of the depletion depth and the wire

† Also at GEC Hirst Research Centre, Wembley, Middlesex HA9 7PP, UK.

0953-8984/90/071807 + 09 $03.50 

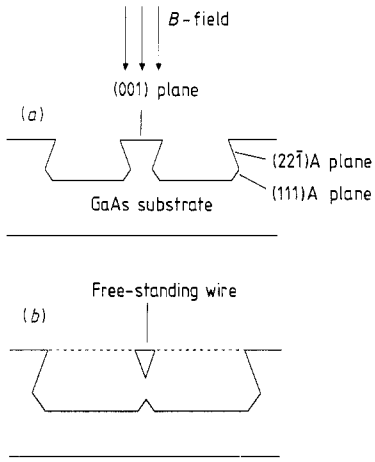


**Figure 1.** (*a*) Etch profile of the citric acid/$H_2O_2$ etch before the mesa becomes free-standing as seen from the $\langle 1\bar{1}0 \rangle$ direction in GaAs; (*b*) etch profile after formation of a free-standing wire.

geometry. For GaAs with a similar doping concentration to that used here, the depletion depth is typically $\simeq 100$ nm although this is generally found to be dependent on the nature of the GaAs surface. On this basis, a wire of width 600 nm would be expected to have a maximum conduction width of $\simeq 250$ nm. Magnetoresistance measurements reported below show that this is indeed the case.

In this paper we will present the results of magnetotransport experiments performed on two samples. The first (sample No 14c) consisted of thirty free-standing wires of length 3.2 $\mu$m arranged in parallel. The average wire width was 600 nm and the conductivity correction at low temperatures was found to correspond to a combination of one-dimensional weak localisation and three-dimensional electron–electron interaction effects as predicted by Al'tshuler and co-workers [13, 14]. The second sample (No 15a) consisted of thirty parallel supported wires of length 10 $\mu$m with a typical wire width of 900 nm and here the localisation fitted a three-dimensional model. The temperature dependence of the phase coherence length $L_\varphi$ was found to differ between the two samples. In the free-standing sample (No 14c) $L_\varphi$ was found to be in close agreement with a $T^{-1/2}$ behaviour characteristic of 3D low-energy electron–electron scattering at low temperatures [15], whereas for the supported sample (No 15a) $L_\varphi$ varied as $T^{-0.66}$ even though the dimensionality of the electron–electron interactions was the same in both cases. We believe this because we are observing a cross-over in sample No 15a between two different temperature dependences.

In a companion paper [16] we have exploited the free-standing geometry of sample No 14c in order to undertake a study of thermal transport processes in low-dimensional systems. This study has demonstrated the importance of heat transfer by electrons as opposed to phonons.

## 2. The fabrication of free-standing GaAs wires

The starting material for the study described here was a semi-insulating GaAs wafer onto which was grown a 1 $\mu$m thick layer of n-type GaAs by molecular beam epitaxy (MBE). The dopant used was silicon at a concentration of $10^{17}$ cm$^{-3}$. This concentration

was chosen so as to avoid the metal–insulator transition (which occurs at a doping concentration of approximately $2 \times 10^{16}$ cm$^{-3}$ in GaAs) while at the same time attempting to minimise the electron contribution to $K(T)$.

The first stage in the fabrication process was the formation of ohmic contacts which also served as bond-pads. In order to do this, a 0.8 $\mu$m thick layer of polymethylmethacrylate (PMMA) resist was spun onto the sample surface and patterned using electron beam lithography. Layers of gold, palladium and germanium were then evaporated onto the sample and the technique of 'lift-off' used to remove unwanted metal and unexposed resist, leaving behind AuPdGe bond-pads only on the regions of the sample surface where the resist had been exposed and developed away. The contacts were then sintered using an electron beam rapid-thermal-annealing (RTA) system to render them ohmic.

The final fabrication step was the creation of the wires themselves. This involved the patterning of a 0.4 $\mu$m thick layer of PMMA resist using electron beam lithography, but this time the resist layer acted as a mask for the patterning of the doped epitaxial GaAs layer by wet chemical etching. The etchant employed was a mixture of citric acid and $H_2O_2$ mixed in a 10 : 1 ratio which has been shown to etch GaAs anisotropically to reveal {221}A and {111}A planes [17]. Figure 1 shows how the etch profile can be used to create free-standing wires by etching the GaAs surface on both sides of a resist bar to create, in the first instance, a mesa-type structure with undercut side-walls. This corresponds to sample No 15a. On further etching these side-walls meet to leave a free-standing wire aligned in the ⟨110⟩ direction on the surface of the sample. The cross-section of the free-standing wire will consequently be triangular with the sides defined by (001), (221)A and $(22\bar{1})$A planes.

At the same time as the wires are fabricated, it is also possible to isolate the device electrically by patterning trenches around the contact pads and ensuring that the etch depth exceeds the thickness of the epitaxial layer. Because the (221)A planes are slow etching, they tend to be smooth, a feature that is advantageous when considering phonon conduction. They also have a tendency to exhibit slowly varying fluctuations in width over distances of several micrometres, possibly as a result of variations in the etch rate. This could arise mainly as a result of the start-up time for the etch, which is significant in comparison with the time taken to complete the etch process and will be sensitive to any changes in the nature of the GaAs surface arising from localised contamination or compositional changes during the sintering stage. These fluctuations are a significant factor in defining the fabrication limits for the process.

## 3. Results and discussion

Electrical measurements were performed in a $^3$He cryostat with a temperature range of 0.35–4.2 K. This cryostat allowed the sample to be placed *in vacuo* and attached by a cold finger to a $^3$He pot. This in turn was connected via a thermal weak link to a larger $^4$He pot. By rotary pumping on first the $^4$He and then the $^3$He it is possible to reach temperatures of 0.45 K. Subsequent diffusion pumping on the $^3$He allowed the base temperature of 350 mK to be reached. The sample resistance was measured using an AC sensing current of 0.1–0.3 nA per wire at a frequency of approximately 68 Hz and a lock-in amplifier to measure the voltage across the sample. The sensing current was chosen to ensure that the voltage across the sample was less than 10 $\mu$V in order to minimise any self-heating effects within the wires. At the temperatures under consideration here,

it is estimated that such a sensing voltage would alter the resistance by less than 0.5% which is less than the error in the measurement of the sample resistance.

The results we shall consider here are for the two samples described earlier, with each sample being connected to four bond-pads in order that four-terminal electrical measurements could be performed. Before undertaking the electrical measurements, both samples were examined in an SEM to try and detect any fractures or defects in the wires and to measure the physical wire width. This inspection showed that of the thirty wires that were fabricated on the supported sample (No 15a) 24 had a mean width of 900 nm, 4 had a width of 600 nm and the remaining 2 had a width of 400 nm. These two smallest wires were also free-standing but their overall contribution to the conductance of the sample is negligible; indeed, given the observed fluctuations in width along each wire in this sample of 50–100 nm it is highly probable that their conducting channels are pinched off. This has been observed to be the case in samples consisting solely of free-standing wires of width 400 nm. In the free-standing sample (No 14c), however, the spread of values for the wire width was much less, probably as a consequence of the reduced wire length. Here 27 of the 30 wires had widths in the range 550–600 nm, one wire was broken and the other two were too thin to conduct. All the wires in this sample were free-standing.

Figure 2 shows how the resistance of the free-standing sample (No 14c) varies with temperature. Here the conductance per unit length per wire (or one-dimensional conductivity) $G(T)$ is plotted as a function of $\ln(T)$ over the range 0.47 K to 10.0 K. The data can be fitted to a relation of the form

$$G(T) = (1.033 + 0.105 \ln T) \times 10^{-10}\ \Omega^{-1}\ \mathrm{m}. \tag{1}$$

Although a $\ln T$ dependence is usually characteristic of two-dimensional behaviour, here it appears to arise from a combination of one-dimensional weak localisation and three-dimensional interaction effects. Magnetoresistance measurements were performed at 15 different temperatures for magnetic fields up to 0.15 T normal to the (001) surface of the wires (see figure 1) and the data fitted to the 1D magnetoconductance theory for the weak localisation régime (equation (2)) of Al'tshuler and Aronov [13]

$$G(B, T) = G_0(T) - (e^2/\pi\hbar)(1/L_\varphi^2 + B^2e^2w^2/3\hbar^2)^{-1/2}. \tag{2}$$

The fitting was performed twice for each temperature. In the first fit the phase coherence length $L_\varphi$ and $w$, the width of the conducting cross-section of each wire perpendicular to the magnetic field, were both treated as variables. This was because in this system due to the depletion depth and the wire shape it was not possible to predict a value for $w$ accurately. However, the fitting procedure yielded a constant width of $125 \pm 15$ nm and a temperature dependent $L_\varphi$. We believe this value of $w$ represents the mean width of the conducting channel; however, due to its triangular shape the channel will be closer to 250 nm wide at the top of the wire and the cross-sectional area of conduction will be approximately $5.0 \times 10^{-14}\ \mathrm{m}^2$. The fitting procedure was then repeated using a constant width of 125 nm in order to obtain a more accurate value for $L_\varphi$. The resulting values for $L_\varphi$ can be fitted to a power law (figure 3) of the form

$$L_\varphi = 181\ \mathrm{nm}(T/\mathrm{K})^{-0.47}. \tag{3}$$

This is close to a $T^{-1/2}$ dependence that is characteristic of three-dimensional low-energy electron–electron scattering [15]. If the localisation term above is subtracted from the 1D conductivity of figure 2 the resulting data have a temperature dependence of the type $a + b\sqrt{T}$ (figure 4). We believe this is due, at least in part, to 3D electron–electron

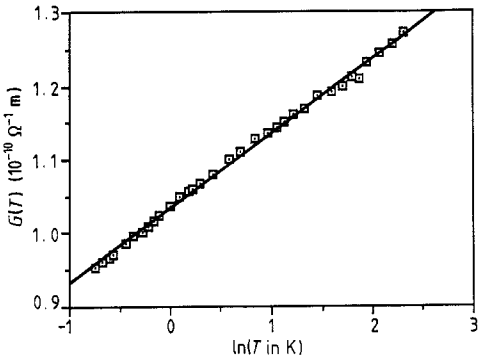


**Figure 2.** A plot of the 1D conductivity $G(T)$ per wire versus ln $T$ for sample No 14c.

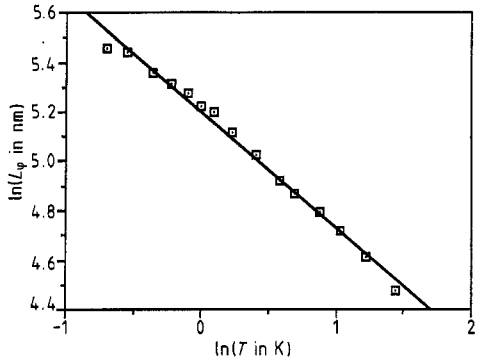


**Figure 3.** $\text{Log}_e$–$\text{log}_e$ plot of the phase coherence length $L_\varphi$ as a function of temperature for sample No 14c.

interactions as predicted by Al'tshuler *et al* [14]. If so, then the data can be fitted to an expression of the form

$$\sigma(T) = \sigma_0 + (1.3e^2/4\sqrt{2}\pi^2\hbar)(\tfrac{4}{3} - \tfrac{3}{2}F_\sigma)(k_B T/D\hbar)^{1/2} \tag{4}$$

where $\sigma_0$ is the 3D conductivity and $D$ is the diffusion constant. The term $F_\sigma$ is a screening parameter related to the Thomas–Fermi screening parameter $F$ by

$$F_\sigma = [32/d(2-d)F][1 + dF/4 - (1 + F/2)^{d/2}] \tag{5}$$

where $d$ is the dimensionality of the system and $F$ is given by

$$F = (1/x)\ln(1 + x) \tag{6}$$

where $x = (2k_F\lambda_{TF})^2$ with Fermi wavevector $k_F$ and $\lambda_{TF}$ the Thomas–Fermi screening length. From this we were able to extract values of $8.21 \times 10^{-5}\ \text{m}^2\ \text{s}^{-1}$ and $2190\ \Omega^{-1}\ \text{m}^{-1}$ for the diffusion constant $D$ and $\sigma_0$ respectively, and hence 25 nm for the thermal (interaction) length $L_T = \sqrt{(D\hbar/k_B T)}$ at 1 K. It should be noted that these values for $D$ and $\sigma_0$ are dependent on the assumed cross-sectional area of each wire. If we calculate $D$ on the basis of $\sigma_0 = De^2 g(E_F)$, where the free-electron-like density of states at the Fermi energy is assumed to take the value $g(E_F) = 4 \times 10^{44}\ \text{J}^{-1}\ \text{m}^{-3}$, we obtain a value of $2.1 \times 10^{-4}\ \text{m}^2\ \text{s}^{-1}$ for the diffusion constant. The difference between these values for $D$ implies that there may be an extra term in addition to the 3D electron–electron interaction term (equation (4)) that contributes to the conductivity increase in figure 4, possibly due to carrier freeze-out. Alternatively there may be a correction to the screening factor $F_\sigma$ as a result of surface depletion and a change in carrier density in the wire. However, both values for $D$ result in a thermal length $L_T$ of less than 40 nm at 1 K which is consistent with the observation of 3D electron–electron interactions.

Although $L_\varphi$ approximates fairly well to a $T^{-1/2}$ dependence, there is a small but significant deviation away from this behaviour below 1 K and towards a $T^{-1/3}$ power law. Such a temperature dependence has been predicted by Al'tshuler *et al* [18] for the

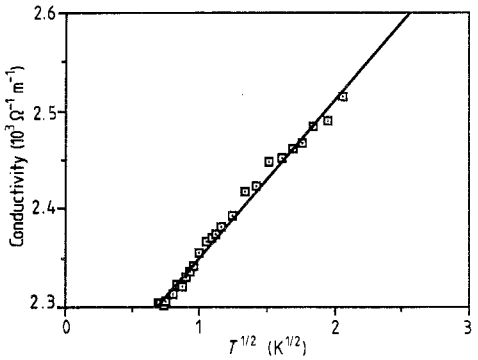


**Figure 4.** A plot of the 3D conductivity versus $\sqrt{T}$ for sample No 14c after subtraction of the 1D localisation contribution.

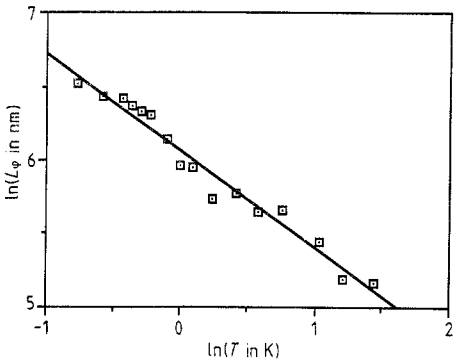


**Figure 5.** $\mathrm{Log_e}$–$\mathrm{log_e}$ plot of the phase coherence $L_\varphi$ as a function of temperature for sample No 15a.

case of 1D electron–electron scattering with small energy transfers ($\Delta\varepsilon \ll kT$). If this is indeed the case then the corrected phase coherence length $L'_\varphi$ should vary as

$$L'_\varphi = L_\varphi(1 - L_\varphi^3/L_N^3\sqrt{2}) \tag{7}$$

where $L_\varphi$ is the dominant phase breaking length (varying as $T^{-1/2}$) and

$$L_N = (DA\sigma_0\hbar^2/2e^2k_BT)^{1/3} \tag{8}$$

is the phase breaking length due to low-energy electron–electron scattering [18]. We have found that equation (7) can give a marginally better fit to the data of figure 3 with an appropriate choice of $L_\varphi$ and $L_N$ but the improvement cannot be considered significant in comparison with the error in experimentally determining $L'_\varphi$ ($\simeq 5\%$).

As well as free-standing wires, electrical measurements have been performed on wires supported on a substrate. As described earlier, sample No 15a consists of 30 wires of length 10 $\mu$m, two of which are in all probability not conducting. The resistance of this sample was measured as a function of temperature over the range 0.47–10 K and again magnetoresistance measurements were performed over the temperature range 0.47–4.2 K. As before, the magnetic field was orientated perpendicular to the (001) plane of the wires and swept over the range $-0.15$ T to $+0.15$ T at 16 different lattice temperatures, and the data fitted to the 3D magnetoconductance theory of Kawabata [19], again in the weak localisation régime. In the low-field limit ($L_B \gg L_\varphi$, where $L_B^2 = \hbar/eB$) the conductivity correction is

$$\Delta\sigma = e^4L_\varphi^3B^2/12\pi^2\hbar^3. \tag{9}$$

From SEM observations of the physical size of the wires, coupled with the observed etch profile and the measured depletion depth, we have estimated the total electrical cross-sectional area of the sample to be $7.7 \times 10^{-12}$ m$^2$, and this has enabled us to determine the following form for $L_\varphi$ (figure 5) using equation (9):

$$L_\varphi = 429\ \mathrm{nm}(T/\mathrm{K})^{-0.66}. \tag{10}$$

As for the free-standing sample (No 14c) the electron–electron interaction term was

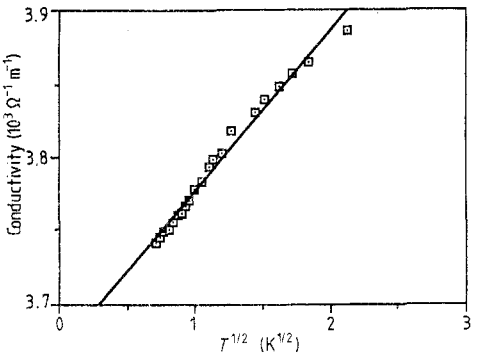


**Figure 6.** A plot of the 3D conductivity versus $\sqrt{T}$ for sample No 15a after subtraction of the 3D localisation contribution.

obtained by subtracting 3D localisation term from the conductance. Again the interaction term appears to be three-dimensional (figure 6) as can be seen from the characteristic $T^{1/2}$ dependence, and we were able to extract values of $2.1 \times 10^{-4}\,m^2\,s^{-1}$ and $3668\,\Omega^{-1}\,m^{-1}$ for $D$ and $\sigma_0$ respectively. However, using $\sigma_0 = De^2g(E_F)$ we again obtain a different value for $D$ compared with that derived from the interaction term, of $3.6 \times 10^{-4}\,m^2\,s^{-1}$. Again this may be due to uncertainty in the area of the conduction cross-section due to the unknown magnitude of the depletion depth at the (221)A planes, or in the calculated value of $F_\sigma$, or we may be observing an extra conductivity correction. However, both values for $D$ result in values for $L_T$ of less than 60 nm at 1 K which is again consistent with our observation that the interactions are three-dimensional.

It can be seen that both $D$ and $\sigma_0$ are a factor of 2 greater than in the free-standing sample (No 14c). This is not entirely unexpected as the wires of that sample are narrower and exhibit 1D localisation. Consequently the electrons in sample No 14c will be more strongly localised and less effectively screened from the static charge in the depletion layer.

Finally, if we return to the temperature dependence of the phase coherence length for the supported wires (equation (10), figure 5) we find that it does not exhibit the usual $T^{-p/2}$ power law (where $p$ is an integer) that is usually encountered. It has been shown by Al'tshuler and Aronov [20, 21] that when $L_\varphi$ is determined by electron–electron collisions with large energy transfers ($\Delta\varepsilon \sim k_BT$) then $L_\varphi$ varies with temperature as $T^{-3/4}$. If this is the dominant scattering mechanism in this system then we would expect to observe a scattering time $\tau_\varphi$ of $\simeq$0.5 ns, and hence a value $\simeq$400 nm for $L_\varphi$ at 1 K. This is in close agreement with our experimentally determined value for $L_\varphi$; the only discrepancy between the two models therefore would appear to be the slight difference in the temperature dependence. One possible explanation for this is that we are observing a transition from a $T^{-3/4}$ to a $T^{-1/2}$ dependence as predicted by Isawa [15]. If so, then $\tau_\varphi$ should vary as

$$1/\tau_\varphi = -[9\pi\sqrt{6\pi\hbar\tau_e}/8(E_F\tau_e)^2]\zeta(-\tfrac{1}{2})(k_BT)^{3/2} + (3\sqrt{3}/4)/\hbar k_BT/(E_F\tau_e)^2 \qquad (11)$$

where $\zeta(-\frac{1}{2}) = -0.2079$. The $T^{3/2}$ and linear $T$ terms will be equal at a transition temperature $T_c$ given by

$$T_c \simeq 0.166\hbar/k_B\tau_e. \qquad (12)$$

For an elastic scattering time $\tau_e \simeq 10^{-13}$ s calculated from $\sigma_0$ above we obtain a value for

$T_c \simeq 14$ K; however, even at temperatures below 4.2 K the $T^{3/2}$ term will still contribute up to 30% of the scattering rate. This would be sufficient to account for the observed deviation from a $T^{-1/2}$ temperature dependence for $L_\varphi$ to the observed $T^{-0.66}$ dependence. For the free-standing sample (No 14c) $\tau_e$ is lower (by a factor of 2) and consequently $T_c$ will be a factor of 2 larger. It is possible therefore that in the free-standing sample we are observing a phase coherence length $L_\varphi$ well below the transition where the $T^{3/2}$ term is less significant. It is also worth noting that the experimental error in $L_\varphi$ will be considerably larger for the supported sample than for the free-standing wires because of the small range of magnetic fields over which equation (9) is valid.

## 4. Summary and implications

We have examined the magnetotransport of two samples consisting of fine $n^+$-GaAs wires of differing sample geometry. In both cases we can interpret the data by invoking a model consisting of electron weak localisation and electron–electron interactions in disordered systems. The free-standing wires (sample No 14c) had a smaller electronic conduction cross-section and consequently exhibited one-dimensional weak localisation, but the electron–electron interactions remained three-dimensional. The supported wires (sample No 15a) had a larger cross-section and here both the localisation and interaction effects were three-dimensional. The magnitude and temperature dependence of the phase coherence length $L_\varphi$ in both samples can be attributed to electron–electron scattering. At this stage we are unable to detect any behaviour that is explicitly due to phonons or the free-standing nature of sample No 14c. This is not surprising as we have used very small sensing currents, so any heating effects in the wires have been minimised.

In a companion paper to this [16] self-heating experiments have been performed on the free-standing wires of sample No 14c (similar to those undertaken by Smith and coworkers [22, 23] on free-standing AuPd wires) in order to determine the temperature dependence of the thermal conductivity $K(T)$. The electron temperature in the wires was calibrated using the one-dimensional electrical conductivity $G(T)$ of equation (1) (figure 2). From the temperature dependence of $K(T)$ it has been possible to establish whether the dominant thermal conduction mechanism is via electron–electron collisions or via the generation of phonons.

These results have implications for future specimen design. Our aim has been to fabricate a structure capable of exhibiting low-dimensional electrical and phonon transport, yet due to the excessive depletion depth and non-uniformities in wire width it has not been possible to fabricate wires with widths below 0.4 $\mu$m that were capable of supporting electrical conduction. Even at these dimensions the structures need to be examined near our experimental limits in order for low-dimensional transport to be observed. One possible solution would be to use material of a higher doping density (say $10^{18}$ cm$^{-3}$) but this, while facilitating the fabrication of smaller free-standing structures will also result in an increased electronic contribution to $K(T)$. A more promising solution would be to adopt silicon as the basis for our study and choose a doping concentration below the Mott transition ($3.7 \times 10^{18}$ cm$^{-3}$) where it is hoped the electron–phonon interaction rate will be more significant. This would, however, require a different approach for the fabrication process [11] as there is no equivalent anisotropic etchant for silicon to compare with the citric acid/$H_2O_2$ system used here.

## Acknowledgments

A Potts, D G Hasko and C G Smith are supported by the Science and Engineering Research Council (UK). A Potts has a CASE Studentship with GEC. M J Kelly holds a Royal Society/SERC Industrial Fellowship.

## References

[1] Taylor R P, Leadbeater M L, Whittington G P, Main P C, Eaves L, Beaumont S P, McIntyre I, Thoms S and Wilkinson C D W 1988 *Surf. Sci.* **196** 52
[2] Dean C C and Pepper M 1982 *J. Phys. C: Solid State Phys.* **15** L1287
[3] Thornton T J, Pepper M, Ahmed H, Andrews D and Davies G J 1986 *Phys. Rev. Lett.* **56** 1198
[4] van Houten H, Beenakker C W J, van Wees B J and Mooij J E 1988 *Surf. Sci.* **196** 144
[5] Chaudhari P and Habermeier H-U 1980 *Solid State Commun.* **34** 687
[6] White A E, Tinkham M, Skocpol W J and Flanders D C 1982 *Phys. Rev. Lett.* **48** 1752
[7] Jäckle J 1981 *Solid State Commun.* **39** 1261
[8] Akkermans E and Maynard R 1985 *Phys. Rev.* B **32** 7850
[9] Kelly M J 1982 *J. Phys. C: Solid State Phys.* **15** L969
[10] Davis J R, McMahon R A and Ahmed H 1985 *J. Electrochem. Soc.* **132** 1919
[11] Potts A, Hasko D G, Cleaver J R A and Ahmed H 1988 *Appl. Phys. Lett.* **52** 834
[12] Hasko D G, Potts A, Cleaver J R A and Ahmed 1988 *J. Vac. Sci. Technol.* B **6** 1849
[13] Al'tshuler B L and Aronov A G 1981 *JETP Lett* **33** 499
[14] Al'tshuler B L, Khmel'nitzkii D, Larkin A I and Lee P A 1980 *Phys. Rev.* B **22** 5142
[15] Isawa Y 1984 *J. Phys. Soc. Japan* **53** 2865
[16] Potts A, Kelly M J, Smith C G, Hasko D G, Cleaver J R A, Ahmed H, Peacock D C, Ritchie D A, Frost J E F and Jones G A C 1990 *J. Phys.: Condens. Matter* **2** 1817
[17] Otsabo M, Oda T, Kumabe H and Miki H 1980 *J. Electrochem. Soc.* **123** 676
[18] Al'tshuler B L, Aronov A G and Khmel'nitzkii D E 1982 *J. Phys. C: Solid State Phys.* **15** 7367
[19] Kawabata A 1980 *Solid State Commun.* **34** 431
[20] Al'tshuler B L and Aronov A G 1979 *JETP Lett.* **30** 482
[21] Al'tshuler B L and Aronov A G 1981 *Solid State Commun.* **38** 11
[22] Smith C G and Wybourne M N 1986 *Solid State Commun.* **57** 411
[23] Smith C G, Ahmed H and Wybourne M N 1987 *J. Vac. Sci. Technol.* B **5** 314